International Journal of Pharmaceutics 424 (2012) 58–66

Contents lists available at SciVerse ScienceDirect

International Journal of Pharmaceutics

journal homepage: www.elsevier.com/locate/ijpharm

Preparation and characterization of paclitaxel-loaded DSPE-PEG-liquid crystalline nanoparticles (LCNPs) for improved bioavailability

Ni Zeng[a,b], Quanyin Hu[a], Zhongyang Liu[a], Xiaoling Gao[c], Rongkuan Hu[d], Qingxiang Song[c], Guangzhi Gu[a], Huimin Xia[a], Lei Yao[c], Zhiqing Pang[a], Xinguo Jiang[a], Jun Chen[a,*], Liang Fang[b,**]

[a] Key Laboratory of Smart Drug Delivery, Ministry of Education & PLA, School of Pharmacy, Fudan University, Lane 826, Zhangheng Road, Shanghai 201203, PR China
[b] Department of Pharmaceutical Science, School of Pharmacy, Shenyang Pharmaceutical University, Shenyang, Liaoning 110016, PR China
[c] Department of Pharmacology, Institute of Medical Sciences, Shanghai Jiaotong University School of Medicine, 280 South Chongqing Road, Shanghai, 200025, PR China
[d] National Laboratory for Physical Sciences at Microscale and School of Life Sciences, University of Science and Technology of China, 96 Jinzhai Rd, Hefei, Anhui 230026, PR China

ARTICLE INFO

Article history:
Received 21 October 2011
Received in revised form 4 December 2011
Accepted 25 December 2011
Available online 8 January 2012

Keywords:
DSPE-PEG-liquid crystalline nanoparticles
Crossed polarized light microscopy
Paclitaxel
Sustained release

ABSTRACT

Lipid-based liquid crystalline nanoparticles (LCNPs) have attracted growing interest as a new drug nanocarrier system for improving bioavailability for both hydrophilic and hydrophobic drugs. In this study, self-assembled LCNPs based on soy phosphatidyl choline and glycerol dioleate, which was known possessing low toxicity and negligible hemolysis, were prepared using poly(ethylene glycol)-grafted 1,2-distearoyl-sn-glycero-3-phosphatidylethanolamine (DSPE-PEG) as the dispersing agent. Paclitaxel (PTX) was used as a model hydrophobic drug. The particle size of the optimized DSPE-PEG-LCNPs and PTX-loaded DSPE-PEG-LCNPs were around 70 nm. Crossed polarized light microscopy was used to characterize the phase behavior of liquid crystalline (LC) matrices, which showed a fan-like birefringent texture in dark background indicating the coexistence of reversed cubic and hexagonal phase in the optimized LC matrix. Transmission electron microscopy and cryo-field emission scanning electron microscopy revealed its internal water channel and "twig-like" surface morphology. PTX-loaded DSPE-PEG-LCNPs exhibited a biphasic drug sustained release pattern with a relatively fast release at the initial stage and a sustained release afterwards. PTX-loaded DSPE-PEG-LCNPs presented higher AUC (410.942 ± 72.522 μg/L h) when compared with commercial product Taxol (212.670 ± 41.396 μg/L h). These results indicated that DSPE-PEG-LCNPs might serve as a potential sustained release system for poorly water-soluble agents.

1. Introduction

In the recent years, lipid-based liquid crystalline nanoparticles (LCNPs) have attracted growing interest as a new drug nanocarrier system due to their potential in improving bioavailability for both hydrophilic and hydrophobic drugs (Gan et al., 2010; Patel et al., 2010; Yaghmur and Michael, 2010; Yang et al., 2004). LCNPs, generally prepared from liquid crystalline (LC) bulk phase by high energy fragmentation methods such as ultrasonication, microfluidization, and homogenization (Yaghmur and Glatter, 2009), was found to form a well-ordered inner structure after dispersing the bulk LC matrices into excess water (Johnsson et al., 2005). The labyrinthine network structures within LCNPs exhibited amazing property for drug delivery by providing protection and sustained release for hydrophilic, hydrophobic and amphipathic drugs that solubilized in LCNPs (Guo et al., 2010).

Commonly encountered lyotropic LC phases were lamellar (L_α), bicontinuous cubic (Q_2) and reversed hexagonal (H_2) phases, and in some particular cases discrete micellar cubic phase (I_2) (Efrat et al., 2007; Nguyen et al., 2010). Among these phases, non-lamellar phases (Q_2 and H_2) were the most studied ones in pharmaceutical area. The Q_2 and H_2 phases possess a thermodynamically stable 3D- or 2D-structure when reconstituted in aqueous environment, providing hydrophilic channels that separated by lipid bilayer (Kaasgaard and Drummond, 2006). Until recently only a limited number of materials have been identified being capable of naturally forming such non-lamellar LC mesophases in excess aqueous solution. However, the two well-known materials, glycerol monooleate (GMO) and phytanetriol (3,7,11,15-tetramethyl hexadecantriol) have been restricted in use of injectable products (Barauskas et al., 2010; Boyd, 2005). According to Barauskas et al. (2010)'s research, GMO-based LCNPs induced hemolysis when mixed with rat whole blood. Phytantriol, restricted by cost in practice, has been wildly used as an ingredient in cosmetics products (Misiūnas et al., 2008) but not in injection ones. Therefore, it is

* Corresponding author. Tel.: +86 21 51980066; fax: +86 21 51980069.
** Corresponding author. Tel.: +86 24 23986330; fax: +86 24 23986330.
E-mail addresses: chenjun@fudan.edu.cn (J. Chen), fangliang2003@yahoo.com (L. Fang).

0378-5173/$ – see front matter © 2012 Elsevier B.V. All rights reserved.
doi:10.1016/j.ijpharm.2011.12.058

of a significant need for developing alternative self-assembled LC systems with higher safety and lower cost.

Recently, a new lipid LC matrix based on soy phosphatidyl choline (SPC) and glycerol dioleate (GDO) (Fig. 1) have been reported (Orädd et al., 1995; Rosenbaum et al., 2010; Tiberg and Fredrik, 2010). It has been demonstrated that LCNPs derived from this SPC/GDO combination presented less hemolytic activity compared with the GMO-based ones (Barauskas et al., 2010). LCNPs based on SPC/GDO/polysorbate 80 (P80) system showed extended terminal half-life for intravenous (i.v.) delivery of both hydrophobic and hydrophilic drugs (Cervin et al., 2008; Johnsson et al., 2006). P80 (Fig. 1), which consist of three short hydrophilic poly (ethylene glycol) (PEG) chains and a hydrophobic oleic acid residue (Daher et al., 2003), was here used as a stabilizing agent for the dispersed LCNPs. Despite their attractive properties in drug delivery, the phase behavior of the SPC/GDO/P80-based LCNPs has not yet been fully understand, which greatly hinder potential application of this system.

For decades, hydrophilic polymers, most notably PEG, were grafted or absorbed to the surface of nanoparticles to provide steric stabilization and "stealth" properties for preventing the nanoparticles from being distinguished and cleared by the mononuclear phagocytic system (MPS) (Avgoustakis, 2004; Otsuka et al., 2003). On the other hand, growing interest has been drawn in the development of functionalized nanoparticulated DDS (Dos Santos et al., 2007; Guo et al., 2011; Li and Huang, 2008; Riviere et al., 2011; Song et al., 2009; Wen et al., 2011) by using bifunctional PEG as hydrophilic outer shell, which enable the conjugation of bioactive ligands to the surface of nanoparticles, and facilitate receptor/absorptive-mediated drug delivery. Poly(ethylene glycol)-grafted 1,2-distearoyl-sn-glycero-3-phosphatidylethanolamine (DSPE-PEG, Fig. 1), whose hydrophobic end can be inserted in the lipidic membrane, while hydrophilic end extend to the surface to form a thin hydrogel layer, has been wildly used in PEGylated formulations (Dos Santos et al., 2007). Base on the similar structure and physicochemical properties between P80 and DSPE-PEG, here we hypothesized that DSPE-PEG might act as an alternative to P80 for serving as a dispersing and stabilizing agent for the SPC/GDO-based LCNPs, which might enable the construction of a stealth and functional LCNPs-based delivery system.

Paclitaxel (PTX) is an effective and widely used anticancer drug in clinical practice. However, due to its low solubility (<1 μg/mL) (Liggins et al., 1997) and low permeability across the intestinal barrier (Yao et al., 2011). PTX is usually administered intravenously through a concentrated solution, trade name Taxol, which contains PTX 6 mg/mL in a mixed solvent composed of cremophor EL and dehydrated alcohol (1:1, v/v). Cremophor EL exhibits a high risk in inducing serious side effects in patients, such as allergic reaction, neurotoxicity, and nephrotoxicity (Kim et al., 2001; Fjuskog et al., 1994; Gelderblom et al., 2001; Lee et al., 2003; Markman et al., 2011; Weiss et al., 1990). Therefore, the development of alternative formulations for PTX is of an urgent requirement.

In this contribution, in order to develop long circulating LCNPs carriers with enabled ligand conjugation property for targeted delivery in the forthcoming future, DSPE-PEG was incorporated in the SPC/GDO/P80 system as an alternative to P80. PTX was used as a model hydrophobic drug. Crossed polarized light microscopy (CPLM) was applied to study the phase behavior of the lyotropic liquid crystals for optimizing the proportion of P80/DSPE-PEG in the LCNPs formulation. LCNPs were prepared using a high pressure. Microfluidizer with the particle distribution determined by dynamic light scattering (DLS). Morphology of nanoparticles was characterized by transmission electron microscopy (TEM) and cryo-field emission scanning electron microscopy (cryo-FESEM). *In vitro* drug release study was conducted using an equilibrium dialysis method to determine the influence of LCNPs on the release behavior of PTX. Finally, *in vivo* pharmacokinetics of PTX that loaded in LCNPs was evaluated to demonstrate the potential utility of this SPC/GDO/DSPE-PEG-based LCNPs system as nanocarriers for hydrophobic agents.

2. Materials and methods

2.1. Materials and animals

Soy phosphatidyl choline (SPC, Lipoid S 100) (containing phosphatidyl choline 95.2%) was purchase from Toshisun (Lipoid, Germany). Glycerol dioleate was obtained from J&K (Beijing, China). Poly(ethylene glycol-2000)-grafted 1,2-distearoyl-sn-glycero-3-phosphatidylethanolamine (DSPE-PEG_{2000}) was synthesized by Nippon Fine Chemical (Osaka, Japan). PTX was purchased from Xi'an Sanjiang Biological Engineering Co. Ltd., and Taxol® from Bristol–Myers Squibb Company. Polysorbate-80 (P80) was from Dazhong Co., Ltd. (Shanghai, China) and Cremophor EL from BASF (Germany). All other reagents were of analytical or chromatographic pure grade and purchased from Sinopharm Chemical Reagent Co., Ltd. (Shanghai, China).

Male Sprague-Dawley rats (200 ± 20 g) were obtained from the Experimental Animal Center of Fudan University and housed at 22 ± 2 °C with access to food and water *ad libitum*. The protocol of animal experiments was approved by the Fudan University Institutional Animal Care and Use Committee.

2.2. Preparation of LCNPs

LCNPs were prepared by using the solvent precursor method as described previously (Rizwan et al., 2011) with minor modification. In all experiments, the SPC: GDO ratio was 50:50 (w/w). Varying amounts of (SPC/GDO), P80, DSPE-PEG and PTX were mixed with the hydrotrope (10% ethanol to the total additives) and stirred for 3 h to form a uniform and clear oil phase. HEPES solution (20 mM HEPES, pH 7.4) (20% to lipid, w/w) was gently added into the lipids, followed by an incubation under stirring at room temperature for at least 24 h (the entrapment of air bubbles was carefully prevented by adjusting the stirring speed) to form a bulk LC matrix. The LC precursor was then injected into HEPES solution under magnetic stirring at 60 °C to form a coarse dispersion. This dispersion was subsequently homogenized using a Microfluidizer (Nano DeBEE, USA) at a pressure of 10,000 psi for 3 cycles and 30,000 psi for 2 cycles.

In this paper, the optimized SPC/GDO/P80-based formulation was hereafter simply referred to as P80-LCNPs and the SPC/GDO/DSPE-PEG-based one was denominated as DSPE-PEG-LCNPs.

2.3. Particles size

The measurement of particle size of LCNPs was performed with dynamic light scattering (PSS NICOMP 380, USA) at 20–25 °C. The particles size distribution (PSD) was characterized by the intensity averaged particle size and polydispersity index (P.I.).

2.4. Crossed polarized light microscopy

Phase behavior of LC mesophases with or without PTX was characterized with crossed polarized light microscopy. One drop of the matrix was added onto a microscope slide, which was then covered with a cover slip. The LC textures were observed under a Zeiss Axiovert 40 MAT microscope (Carl Zeiss, Oberkochen, Germany)

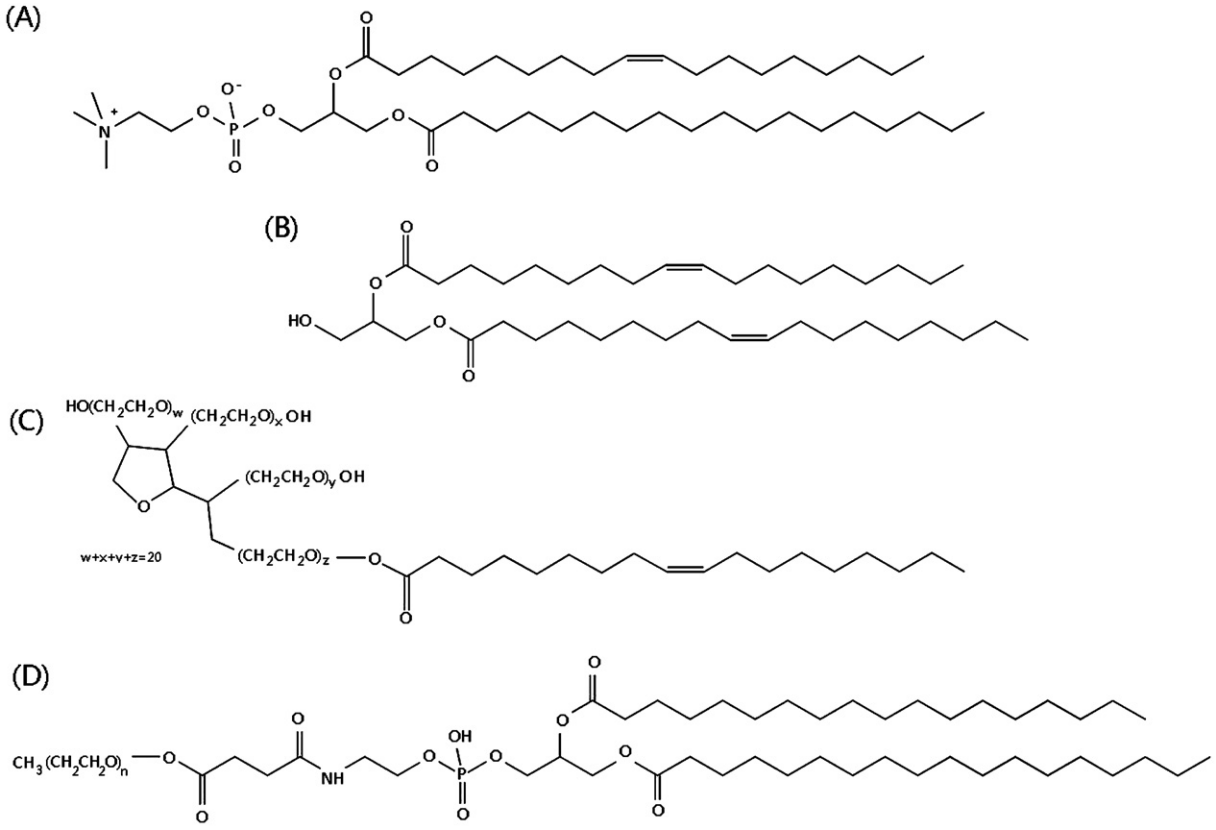

Fig. 1. Molecular structures of LCNPs: (A) SPC; (B) GDO; (C) P80; (D) DSPE-PEG.

that fitted with an AxioCam camera at ambient temperature. A magnification of ×200 was used.

2.5. Transmission electron microscopy

The morphological examination of LCNPs was performed with transmission electron microscopy (H-600, Hitachi, Japan) following negative staining with sodium phosphotungstate solution.

2.6. Cryo-field emission scanning electron microscopy

The surface morphology of LCNPs was visualized by cryo-field emission scanning electron microscopy (Hitachi, S-4800, Japan). The samples were frozen with liquid nitrogen, transferred into the cryo stage (Gatan, Alto 2500, UK) of the microscope, sputtered with gold to provide a conductive coating, and examined at −100 °C.

2.7. Encapsulating efficiency, drug loading capacity and in vitro drug release

The encapsulating efficiency (EE%) and loading capacity (LC%) of PTX in P80-LCNPs and DSPE-PEG-LCNPs was determined by gel filtration chromatography as described previously (Lai et al., 2009). The eluate containing LCNPs was dissolved in methanol to release PTX. The PTX content was determined with Shimadzu LC-10AT HPLC system (Shimadzu, Japan) using a reverse phase C-18 Diamonsil column (4.6 mm × 200 mm, 5 μm, Dikma, China) with methanol/water (75/25 v/v) as the mobile phase at the flow rate of 1.2 mL/min. The column temperature was maintained at 40 °C, sample injection volume was 20 μL and the detection wavelength was 227 nm. The EE% and LC% were calculated as indicated below ($n = 3$).

$$\text{EE\%} = \frac{\text{PTX in cubic nanoparticles}}{\text{total amount of PTX in dispersion}} \times 100\% \quad (1)$$

$$\text{LC\%} = \frac{\text{PTX in cubic nanoparticles}}{\text{nanoparticles weight}} \times 100\% \quad (2)$$

In vitro drug release was performed using an equilibrium dialysis method (Boyd, 2005). Briefly, 1 mL of the freshly prepared LCNPs suspension (equivalent to 30 μg drug) was added in a sealed dialysis bag (molecular weight cut off 9 kDa), which was then immersed in 30 mL release medium (HEPES solution with 0.1% (v/v) P80 for providing sink condition throughout the release test) and incubated at 37 °C at the shaking speed of 100 rpm. At time intervals (0, 0.5, 1, 2, 3, 4, 6, 8, 16, 24, 48, 72 and 96 h), 200 μL of the release sample was withdrawn and immediately equal amounts of fresh dissolution medium were replenished. Samples were analyzed using the HPLC method as mentioned above.

To evaluate the release mechanism of PTX-loaded LCNPs, drug release was plotted against the square root of time, which could be described by the Higuchi diffusion equation given by:

$$Q = [D_m C_d (2A - C_d)t]^{1/2} \quad (3)$$

where Q is the mass of drug released at time t, and is proportional to the apparent diffusion coefficient of the drug in the matrix D_m, the initial amount of drug in the matrix A, and the solubility of the drug in the matrix C_d (Boyd, 2003; Boyd et al., 2006a; Higuchi, 1967).

2.8. In vivo pharmacokinetics

In order to evaluate the potential application of DSPE-PEG-LCNPs as nanocarriers for hydrophobic agents, *in vivo*

pharmacokinetics of PTX-loaded P80-LCNPs and DSPE-PEG-LCNPs were conducted in Sprague-Dawley rats after vein injection. The rats were randomly divided into three groups, and injected with Taxol, PTX-loaded P80-LCNPs and DSPE-PEG-LCNPs, respectively, at the PTX dose of 1 mg/kg. At the time points (0.083, 0.25, 0.5, 1, 2, 3, 4, 6, 8, 12 and 24 h) after administration, blood was collected into the tube with heparin. Plasma was collected following centrifugation and stored at −20 °C until analysis.

To prepare samples for analysis, 90 μL methanol containing 60 ng/mL docetaxol (internal standard) was added to 30 μL plasma to precipitate the proteins. The mixture was vortexed and subsequently centrifuged at 12,000 rpm for 10 min with the supernatant mixed with an equal volume of deionized water and subjected to liquid chromatography-tandem mass spectrometry (LC–MS/MS) analysis. Chromatography was performed using an Agilent 1100 HPLC system with a Gemini C18 column (100 mm × 2.0 mm i.d., 3.0 μm, Phenomenex, Torrance, CA, USA) at a temperature of 40 °C and a flow rate of 0.3 mL/min using 0.1% formic acid: methaol (3:7) as the mobile phase. Five microliters of the sample was injected for analysis. Mass spectrometric detection was performed on an API 3000 triple quadrupole instrument (Applied Biosystems, Toronto, Canada) in multiple reaction monitoring (MRM) mode. A TurboIon-Spray ionization (ESI) interface in positive ionization mode was used. Data processing was performed with Analyst 1.4.1 software package (Applied Biosystems). The spray voltage was at 5000 V, ion source temperature at 500 °C and collision energy at 30 eV. Detection of the ions was conducted in the multiple reaction monitoring mode, monitoring the transition of the m/z 876.6 → 308.0 for paclitaxel $(M+Na)^+$ and 830.3 → 549.1 for docetaxel $(M+Na)^+$, respectively. All the concentration data were dose-normalized and plotted as plasma drug concentration–time curves.

The pharmacokinetic analysis was performed by means of a model independent method. The terminal elimination rate constant (k) was determined by least-square regression analysis of terminal log-linear portions of the plasma concentration–time profile ($k = -2.303 \times$ slope). The elimination half-life ($T_{1/2}$) was calculated as $0.693/k$. The area under the curve to the last measurable concentration (AUC_{0-t}) was calculated by the linear trapezoidal rule. The area under the curve extrapolated to infinity ($AUC_{0-\infty}$) was calculated as $AUC_{0-t} + Ct/k$, where as Ct is the last measurable concentration. The clearance was calculated as X_0/AUC, and MRT by dividing AUMC by AUC.

2.9. Statistical analysis

All the data were expressed as mean ± standard deviation (SD). Comparison among three groups was performed by one-way ANOVA followed by Bonferroni tests and that between two groups was determined by Student's t-test. Statistical significance was defined as $P < 0.05$.

3. Results

3.1. Characterization of phase behavior

According to SPC/GDO/water ternary phase diagram (Orädd et al., 1995; Rosenbaum et al., 2010; Tiberg and Fredrik, 2010), SPC/GDO (50:50) was chosen as the basic formulation for lipid-based LC phase, which formed I_2 and H_2 when absorbing 10–30 wt% water. Here, phase behavior of the SPC/GDO system with different amount of P80 or DSPE-PEG was characterized with CPLM.

As illustrated in Fig. 2A and Table 1, the interconversion of LC phases occurred when a third miscible component was added. When increasing concentration of P80 in the SPC/GDO-based system from 10% to 50% (w/w), a L_α phase → H_2 and I_2 multiphase → L_α phase transition was observed. When adding P80 to 25%, a bright fan-like texture in isotropic dark background was observed, together with high viscosity of the sample, indicating the coexistence of reversed cubic and hexagonal phase (H_2 and I_2). Hence, SPC/GDO system with 25% P80 was determined as an optimized P80-LCNPs formulation for further studies.

Table 1
Physical characterization of LCNPs with different amount of P80 in the total additives.

P80%	Phase behavior	Particle size	P.I.
10.0%	L_α	155.5 ± 97.4 nm (63.90%)	0.408
12.5%	$L_\alpha \rightarrow H_2$	154.2 ± 98.4 nm (63.80%)	0.407
16.7%	H_2	114.5 ± 69.2 nm (60.50%)	0.366
20.0%	$H_2 \rightarrow I_2$	93.0 ± 57.2 nm (61.50%)	0.378
25.0%	H_2 and I_2	89.8 ± 54.9 nm (61.10%)	0.373
33.5%	H_2 and $I_2 \rightarrow L_\alpha$	55.9 ± 38.2 nm (68.30%)	0.366
50.0%	H_2 and $I_2 \rightarrow L_\alpha$	64.3 ± 57.7 nm (80.50%)	0.648

In order to construct a functional LCNPs-based delivery system, different amount of DSPE-PEG was incorporated into the optimized SPC/GDO/P80 system (Fig. 2B, Table 2). A H_2 and I_2 multiphase to L_α phase transition was observed when DSPE-PEG started to incorporate with the SPC/GDO/P80/water system. When P80 was almost completely replaced by DSPE-PEG (90–100%) in the SPC/GDO/P80 matrix, non-lamellar LC phase (H_2 and I_2) was observed again. Based on CPLM results of the precursor phases, SPC/GDO system with 25% DSPE-PEG without P80 was determined to be the optimized DSPE-PEG-LCNPs formulation.

3.2. Particle size distribution

The particle size of LCNPs with P80 from 10% to 50% was summarized in Table 1. These results showed reduced particle size of P80-LCNPs with increased amount of P80. While the phase transition ($I_2 \rightarrow L_\alpha$) at 50.0% of P80 appeared to produce slightly larger particles (64.3 nm, P.I. 0.648). On the other hand, the particle size of LCNPs when incorporated with different amount of DSPE-PEG showed good correlation with phase behavior (Table 2), with smaller particle sizes derived from non-lamellar matrix (H_2 and I_2) but larger ones from L_α matrix. As shown in Table 3, the particle size of the optimized P80-LCNPs and DSPE-PEG-LCNPs formulations (around 70 nm) was slightly increased after the incorporation of PTX (around 80 nm). In addition, LC matrix with 25% DSPE-PEG produced smaller particles than that with 25% P80 (Table 3, Fig. 3).

3.3. Transmission electron microscopy and cryo-field emission scanning electron microscopy

Morphology of P80-LCNPs and DSPE-PEG-LCNPs was characterized with TEM. As shown in Fig. 4, the formed nanoparticles presented spherical flower-like structure with internal water channel as well as external hydrogel layers. Slightly smaller than that showed by DLS, the majority diameters of P80-LCNPs and DSPE-PEG-LCNPs were in the range of 50–80 nm. The thickness of

Table 2
Physical characterization of LCNPs with different amount of DSPE-PEG in the combination of P80/DSPE-PEG.

DSPE-PEG%	Phase behavior	Particle size	P.I.
0%	H_2 and I_2	90.5 ± 57.0 nm (63.00%)	0.397
10.0%	$H_2 \rightarrow L_\alpha$	85.4 ± 52.3 nm (61.20%)	0.375
25.0%	L_α	144.9 ± 107.8 nm (74.40%)	0.554
50.0%	L_α	133.2 ± 60.4 nm (64.80%)	0.520
75.0%	$L_\alpha \rightarrow H_2$	112.7 ± 80.0 nm (71.00%)	0.504
90.0%	H_2 and I_2	96.2 ± 67.4 nm (70.10%)	0.491
100.0%	H_2 and I_2	74.1 ± 46.2 nm (62.30%)	0.388

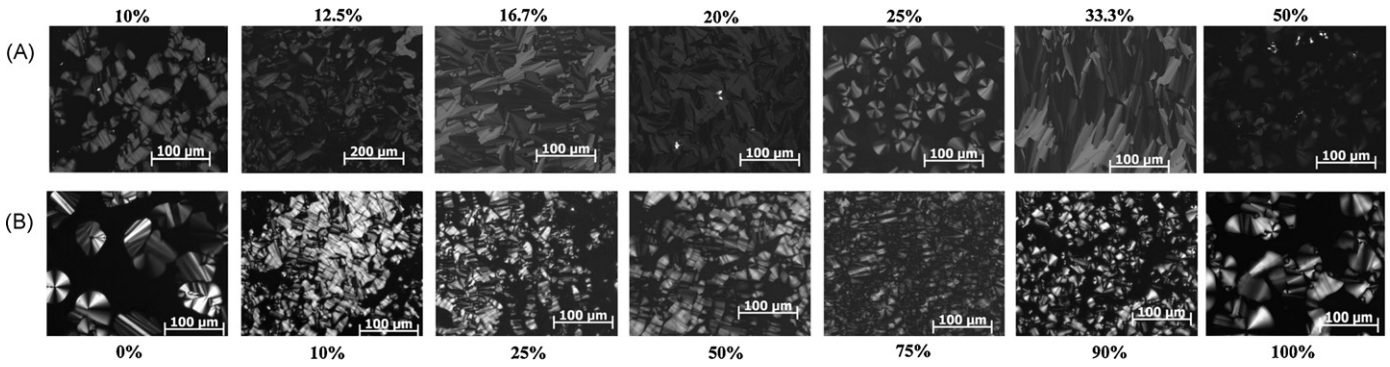

Fig. 2. Photomicrographs of bulk lipid crystalline matrices under crossed polarized light microscopy. (A) Phase behavior of SPC/GDO system with different amount of P80 (10%, 12.5%, 16.7%, 20%, 25%, 33.3%, and 50%); (B) phase behavior of SPC/GDO/P80 system with different amount of DSPE-PEG, the amount of surfactants(P80/DSPE-PEG) is 25% of the total additives, and percentage of DSPE-PEG in the total surfactants are from 0%, 10%, 25%, 50%, 75%, 90%, and 100%.

Table 3
Intensity averaged particle size, polydispersity index, encapsulating efficiency and loading capacity of the optimized LCNPs formulations. Each value represents mean ± SD ($n = 3$).

Formulation	Particle size	P.I.	EE%	LC%
P80-LCNPs	76.33 ± 1.19 nm	0.365 ± 0.014		
DSPE-PEG-LCNPs	63.43 ± 9.52 nm	0.324 ± 0.053		
PTX-loaded P80-LCNPs	84.70 ± 5.26 nm	0.370 ± 0.016	76.91 ± 11.48	0.44 ± 0.03
PTX-loaded DSPE-PEG-LCNPs	74.13 ± 5.44 nm	0.328 ± 0.053	75.69 ± 2.13	0.46 ± 0.02

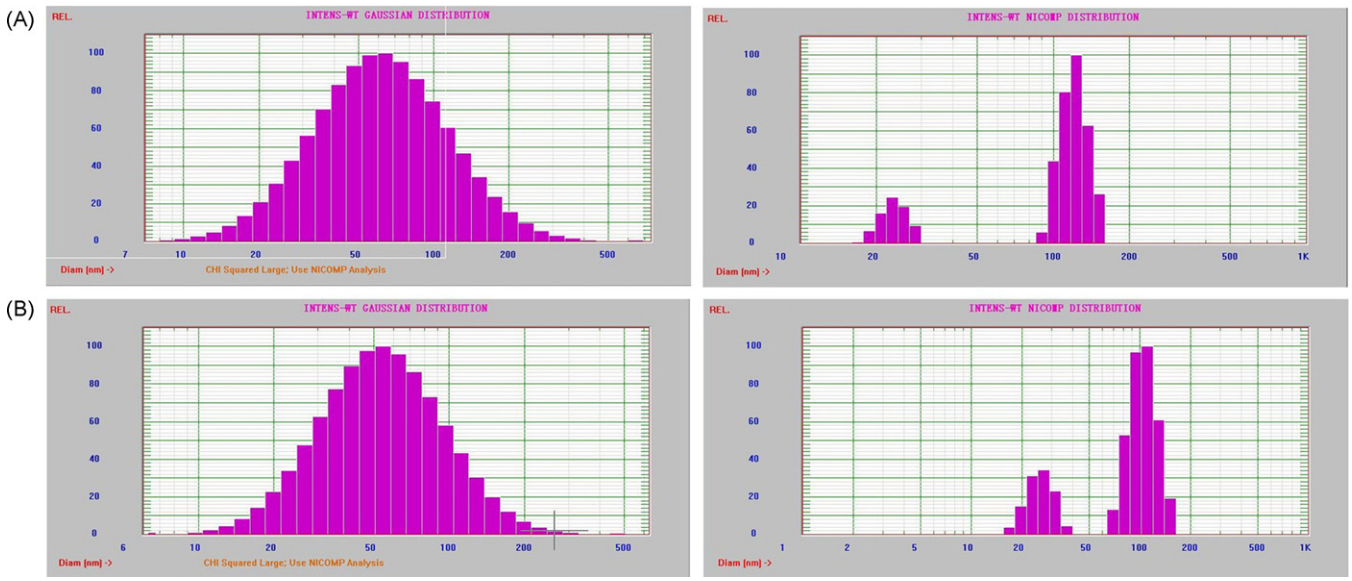

Fig. 3. Particle size of P80-LCNPs (A) and DSPE-PEG-LCNPs (B) when fit to GAUSSIAN (left) and NICOMP (right) distribution, respectively.

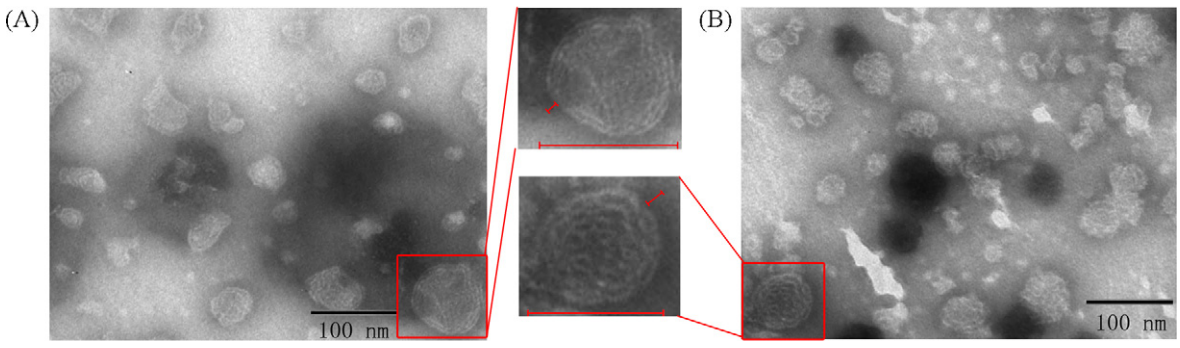

Fig. 4. TEM images of P80-LCNPs (A) and DSPE-PEG-LCNPs (B).

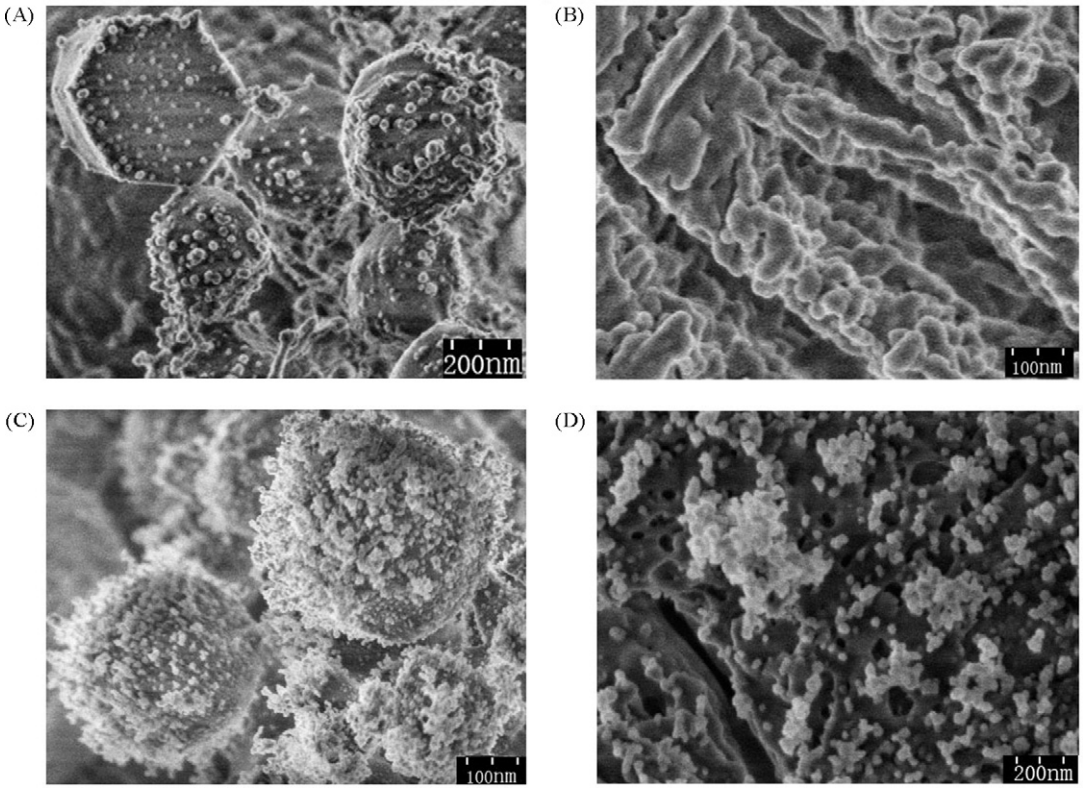

Fig. 5. Cryo-FESEM images of P80-LCNPs and DSPE-PEG-LCNPs: (A) P80-LCNPs; (B) surface morphology of P80-LCNPs; (C) DSPE-PEG-LCNPs; (D) surface morphology of DSPE-PEG-LCNPs.

hydrogel layer of P80-LCNPs and DSPE-PEG-LCNPs was 7–9 nm and 9–11 nm, respectively.

Cryo-FESEM was performed to further characterize the surface morphology of P80-LCNPs and DSPE-PEG-LCNPs. The reversed micellar cubic phase particles exhibited a "ball-like" morphology while the hexosome displayed clear hexagonal structures (Fig. 5A). The P80-LCNPs were found comprised of an internal nanostructured phase with enclosed water channels (Fig. 6B) and a relatively smooth but actually quite rough nodule-like appearance (data not shown). Whereas, the DSPE-PEG-LCNPs possessed a surface structure with a "twig-like" corona, which was speculated to form under −100 °C by the water-bonding hydrophilic PEG chains that protruded toward the external aqueous environment.Encapsulating efficiency, drug loading capacity and *in vitro* drug release

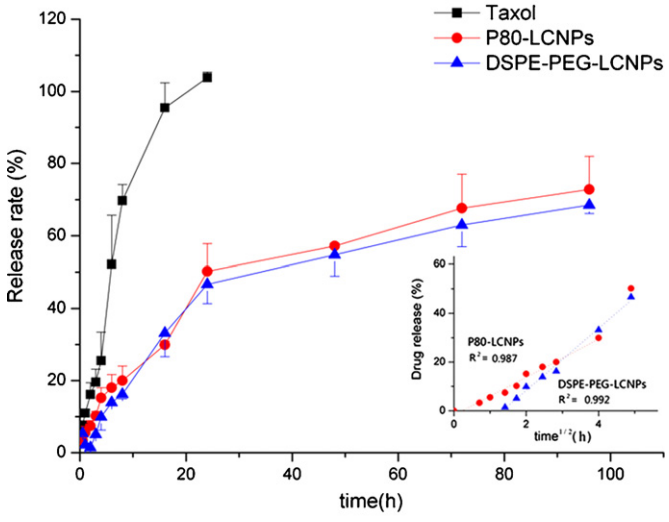

Fig. 6. PTX release from Taxol, P80-LCNPs, and DSPE-PEG-LCNPs in pH 7.4 HEPES buffer at 37 °C ($n = 3$). The initial PTX concentration was 30 μg/mL. On the right corner, dashed lines indicate linear fits to release profiles.

No significant difference in EE (75%) and LC (0.45%) was observed between PTX-loaded P80-LCNPs and DSPE-PEG-LCNPs (Table 3). An equilibrium dialysis method was applied to determine the *in vitro* release behavior of the PTX-loaded P80-LCNPs and DSPE-PEG-LCNPs to evaluate the impact of labyrinthine nanostructures on drug release. In the case of Taxol, complete release was obtained after 16 h. But in the case of PTX-loaded P80-LCNPs and DSPE-PEG-LCNPs, a sustained biphasic drug release, composed of a relative fast drug release in first 24 h (50% release) and a slower one in the following 72 h (70% release totally), was obtained. Furthermore, PTX-loaded DSPE-PEG-LCNPs was found to possess better sustained effect than PTX-loaded P80-LCNPs.

In order to infer the mechanism of PTX release from LCNPs, data from the release studies were plotted as release% *vs.* square root of time (Eq. (3), Fig. 6 right corner). During the initial 16 h, drug release from P80-LCNPs and DSPE-PEG-LCNPs was found well correlated with the square-root of time. The slope for P80-LCNPs and DSPE-PEG-LCNPs were 7.804 and 12.726 $h^{-1/2}$, respectively, indicating a faster diffusion of PTX from DSPE-PEG-LCNPs than that from P80-LCNPs. However, a lag time of 1 h in DSPE-PEG-LCNPs was observed.

3.4. *In vivo* pharmacokinetics

To investigate the *in vivo* fate of the PTX-loaded LCNPs formulations, nine Sprague-Dawley rats were divided into three groups and given intravenously with Taxol, PTX-loaded P80-LCNPs and DSPE-PEG-LCNPs, respectively. Fig. 7 illustrated the pharmacokinetic profiles of PTX obtained after administration. The pharmacokinetic parameters derived from these profiles, namely $C_{5\,min}$, Cl,

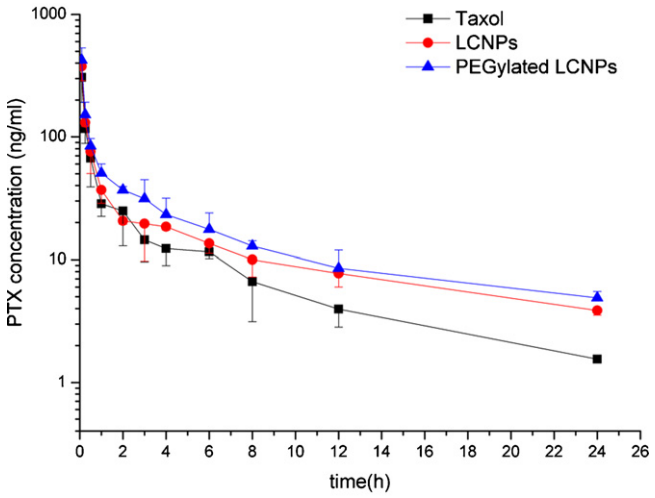

Fig. 7. Plasma PTX profiles after i.v. administration of Taxol, PTX-loaded P80-LCNPs and PTX-loaded DSPE-PEG-LCNPs formulations to Sprague-Dawley rats at the dose of 1 mg/kg PTX ($n = 3$).

$T_{1/2}$, MRT (0–24), MRT (0–∞), AUC (0–24), and AUC (0–∞) were summarized in Table 4. It was found that Taxol resulted in a mean $C_{5\,min}$ of 307.0 ng/mL and $T_{1/2}$ of 4.057 h. In comparison, higher plasma levels were observed for both PTX-loaded P80-LCNPs and DSPE-PEG-LCNPs over the same time scale ($C_{5\,min}$ 377.0 ng/mL, $T_{1/2}$ 8.838 h for the PTX-loaded P80-LCNPs and $C_{5\,min}$ 424.3 ng/mL, $T_{1/2}$ 12.619 h for the PTX-loaded DSPE-PEG-LCNPs). The AUC (0–24) of PTX-loaded P80-LCNPs and DSPE-PEG-LCNPs were 317.030 ± 67.185 μg/L h and 410.942 ± 72.522 μg/L h, respectively, which was approximately 1.5- and 1.9-times as much as that of Taxol (212.670 ± 41.396 μg/L h).

4. Discussion

The aim of this study was to develop DSPE-PEG incorporated LCNPs based on SPC/GDO system which was known possessing low toxicity and negligible hemolysis (Barauskas et al., 2010). Compared with P80-LCNPs, the thicker PEG hydrogel layer in DSPE-PEG-LCNPs might facilitate a better stealth effect *in vivo* and enable the conjugation of bioactive ligands to construct a functional LCNPs-based delivery system. According to previous studies (Boyd, 2005; Kossena et al., 2004), the discrete lipidic hydrophobic and aqueous hydrophilic domains within LCNPs allows diffusion-controlled release for hydrophobic, hydrophilic and amphiphilic molecules. However, most of the reported release studies were restricted to bulk LC matrices (Lee et al., 2009; Clogston et al., 2005; Clogston and Caffrey, 2005; Lee and Kellaway, 2000; Rizwan et al., 2009). Furthermore, the potential of LCNPs as drug carriers has not been fully explored, especially their *in vivo* application. Here the phase behavior of LCNPs, which was modulated by P80 or DSPE-PEG, was examined under CPLM. *In vitro* release and *in vivo* pharmacokinetics of the PTX-loaded P80-LCNPs and DSPE-PEG-LCNPs were performed to evaluate DSPE-PEG-LCNPs as a new drug delivery carrier.

CPLM has a long history of being applied for studying the phase behavior of LC. Under CPLM, the lamellar phase exhibits a distinct woven structure and/or a mosaic or Maltese cross pattern, the hexagonal phase shows a fanlike and angular texture, whereas the isotropic cubic phase only displays a black background without birefringence (Borne et al., 2000; Boyd et al., 2006b; Giddi et al., 2007). In our study, a birefringent fan-like texture in dark environment was observed when the amount of P80 in the SPC/GDO matrix was 25%, indicating the coexistence of reversed cubic phase and hexagonal phase (H_2 and I_2). Thus, SPC/GDO with 25% P80 was determined as an optimized formulation for P80-LCNPs. Coexistence of H_2 and I_2 was also observed at the complete replacement of P80 by DSPE-PEG in the SPC/GDO/P80/water system. As a result, SPC/GDO with 25% DSPE-PEG was determined as the optimized DSPE-PEG-LCNPs formulation. No change in the birefringent texture of P80-LCNPs and DSPE-PEG-LCNPs were found in the presence of PTX (0.5% in the total additives) in the LC matrices (data not shown), indicating that no phase conversion occurred with the incorporation of PTX.

DLS showed that the constructed P80-LCNPs and DSPE-PEG-LCNPs presented small particle size (60–90 nm) and relative wide size distributions (P.I.: 0.320–0.380). In consistent with previous work (Wörle et al., 2007), the LCNPs dispersions displayed bimodal polydisperse population with two distribution (around 100 nm and 25 nm) when fit to NICOMP distribution (Fig. 3). The particle distribution pattern was confirmed by our TEM data (Fig. 4), in which quite a few small particles (around 20 nm) were observed in both the P80-LCNPs and DSPE-PEG-LCNPs formulations. As reported previously (Gaumet et al., 2008), the particle size observed under TEM was found slightly smaller than that of the DLS data. Cryo-FESEM seemed to yield somewhat larger diameters than DLS and TEM, which we believed was resulted from particle aggregation or water channel swelling at −100 °C.

Both P80 and DSPE-PEG are PEG-derivatized polymers (Fig. 1). Their similar amphiphilic structures indicate the similar capacity in facilitating particle dispersion and stabilization. In terms of configuration, the headgroup part of DSPE-PEG is about 3 times as long as that of P80, therefore DSPE-PEG is expected to be more water miscible, which was evidenced by the lower energy input needed for DSPE-PEG-LCNPs during the homogenizing procedure. The thicker PEG hydrogel layer in DSPE-PEG-LCNPs (Fig. 5A and C) made LC mesophase also easier to disperse into excess water when compared with that in P80-LCNPs.

Despite their potential as sustained release carrier, there were still a number of studies that claimed LCNPs should be classified as burst release system (Boyd, 2003, 2005; Boyd et al., 2006a,b). This major limitation of the application of LCNPs was speculated relate to the increased surface area when dispersed into excess

Table 4
Pharmacokinetic parameters for PTX after i.v. administration of Taxol, PTX-loaded P80-LCNPs and PTX-loaded DSPE-PEG-LCNPs to Sprague-Dawley rats (mean ± SD, $n = 3$).

	Taxol	PTX-loaded P80-LCNPs	PTX-loaded DSPE-PEG-LCNPs
$C_{5\,min}$ (μg/L)	307.0 ± 116.1	377.0 ± 88.27	424.3 ± 109.3*
Cl (L/h kg)	4.366 ± 1.000	2.742 ± 0.478	2.016 ± 0.109*
$T_{1/2}$ (h)	4.057 ± 0.489	8.838 ± 3.040	12.619 ± 2.648**
MRT (0–24)(h)	2.906 ± 0.127	5.157 ± 1.609	5.938 ± 0.646**
MRT (0–∞) (h)	4.829 ± 0.495	9.402 ± 2.936	8.114 ± 1.179*
AUC (0–24) (μg/L h)	212.670 ± 41.396	317.030 ± 67.185	410.942 ± 72.522*
AUC (0–∞) (μg/L h)	236.352 ± 47.978	372.738 ± 69.631*	500.452 ± 59.107**

* $P < 0.05$, significantly different from that of the Taxol group.
** $P < 0.01$, significantly different from that of the Taxol group.

water (Garg et al., 2007). In this study, both P80-LCNPs and DSPE-PEG-LCNPs carriers exhibited sustained *in vitro* PTX release. It can be observed that, the release of PTX from P80-LCNPs and DSPE-PEG-LCNPs showed a diffusion controlled release as obeyed Higuchi diffusion equation (Eq. (3)) at the initial stage (during approximately 16 h), and displayed a slower release afterwards. The initial faster release was derived from drug located at the outer layer of the particles while the later slower one from that incorporated in the nanoparticle core and released in a prolonged way *via* the erosion or degradation of the matrix. The same release tendency of PTX from P80-LCNPs and DSPE-PEG-LCNPs at the later 72 h implied similar internal hierarchical structures for PTX encapsulation. However, a subtle difference was observed between the release of PTX from P80-LCNPs and DSPE-PEG-LCNPs at early time points, with a lag time of 1 h in DSPE-PEG-LCNPs and different diffusion coefficients ($12.726\ h^{-1/2}$ in DSPE-PEG-LCNPs *vs.* $7.804\ h^{-1/2}$ in P80-LCNPs). The observed lag time was believed relate to the partitioning of the lipophilic PTX from the lipid regions to the PEG shell and then into release medium, which could be made slower by the "twig-like" hydrogel layer of DSPE-PEG-LCNPs (Fig. 5).

As shown in Table 4, the clearance rate of the PTX formulations followed the order: Taxol, PTX-loaded P80-LCNPs, and PTX-loaded DSPE-PEG-LCNPs. The bioavailability of PTX-loaded DSPE-PEG-LCNPs was significant higher than that obtained of Taxol. In the meanwhile, although not statistically significant, PTX-loaded P80-LCNPs showed improved pharmacokinetic parameters when compared with Taxol, especially the $AUC_{(0-\infty)}$. Together with the results from the *in vitro* release and *in vivo* pharmacokinetics, the noticeably protective effect of DSPE-PEG-LCNPs could be explained by two reasons: firstly, the enhanced "stealth" effect (Alexis et al., 2008; Cui et al., 2011; Li and Huang, 2008) of DSPE-PEG-LCNPs by their longer PEG chains might contribute to higher plasma levels and longer half life in systemic circulation compared with that of P80-LCNPs (Fig. 5A and C). It is generally believed that the surface-grafted PEG shell can reduce plasma protein binding for solid particles surfaces, thereby prolonging circulation lifetimes (Maechling-Strasser et al., 1989; Mori et al., 1982; Otsuka et al., 2003; Cullis et al., 1998; Woodle and Lasic, 1992). Secondly, the difference in particle size between P80-LCNPs (85.8 nm, P.I. = 0.362, with 158.9 ± 13.6 nm (69.20%) in NICOMP distribution) and DSPE-PEG-LCNPs (55.8 nm, P.I. = 0.288, with 88.8 ± 9.1 nm (74.20%) in NICOMP distribution) might also affect the pharmacokinetic profiles. As is well known, smaller particles are more slowly cleared from systemic circulation than the larger ones (Müller et al., 2001). Therefore, the thicker PEG hydrogel layer and smaller particle size of DSPE-PEG-LCNPs might be the major contributors to their slower clearance.

5. Conclusion

PTX-loaded DSPE-PEG-LCNPs carriers for i.v. delivery were prepared in this study. DSPE-PEG was served as an alternative stabilizing agent to P80 for the dispersed LCNPs. The PTX-loaded DSPE-PEG-LCNPs exhibited a similar biphasic sustained release pattern as PTX-loaded P80-LCNPs in the *in vitro* release study but showed much higher AUC and slower clearance compared with Taxol in the *in vivo* pharmacokinetic study. The results together indicated that DSPE-PEG-LCNPs might serve as potential nanocarriers for enhancing i.v. bioavailability of poorly water-soluble drugs.

Acknowledgments

This work was supported by National Natural Science Foundation of China (30801439, 30801442) and grants from Shanghai Science and Technology Committee (10QA1404100, 11430702200).

References

Alexis, F., Pridgen, E., Molnar, L.K., Farokhzad, O.C., 2008. Factors affecting the clearance and biodistribution of polymeric nanoparticles. Mol. Pharm. 5, 505–515.
Avgoustakis, K., 2004. Pegylated poly(lactide) and poly(lactide-co-glycolide) nanoparticles: preparation, properties and possible applications in drug delivery. Curr. Drug Deliv. 1, 321–333.
Barauskas, J., Cervin, C., Jankunec, M., Spandyreva, M., Ribokaite, K., Tiberg, F., Johnsson, M., 2010. Interactions of lipid-based liquid crystalline nanoparticles with model and cell membranes. Int. J. Pharm. 391, 284–291.
Borne, J., Nylander, T., Khan, A., 2000. Microscopy, SAXD, and NMR studies of phase behavior of the Monoolein-Diolein-Water system. Langmuir 16, 10044–10054.
Boyd, B.J., 2003. Characterisation of drug release from cubosomes using the pressure ultrafiltration method. Int. J. Pharm. 260, 239–247.
Boyd, B.J., 2005. Controlled release from cubic liquid-crystalline particles (cubosomes). In: Lynch, M.L., Spicer, P.T. (Eds.), Bicontinuous Liquid Crystals. CRC Press Inc., Florida, pp. 285–305.
Boyd, B.J., Whittaker, D.V., Khoo, S.M., Davey, G., 2006a. Lyotropic liquid crystalline phases formed from glycerate surfactants as sustained release drug delivery systems. Int. J. Pharm. 309, 218–226.
Boyd, B.J., Whittaker, D.V., Khoo, S.M., Davey, G., 2006b. Hexosomes formed from glycerate surfactants-Formulation as a colloidal carrier for irinotecan. Int. J. Pharm. 318, 154–162.
Cervin, C., Vandoolaeghe, P., Nistor, C., Tiberg, F., Johnsson, M., 2008. A combined in vitro and in vivo study on the interactions between somatostatin and lipid-based liquid crystalline drug carriers and bilayers. Eur. J. Pharm. Sci. 36, 377–385.
Clogston, J., Caffrey, M., 2005. Controlling release from the lipidic cubic phase. Amino acids, peptides, proteins and nucleic acids. J. Control. Release 107, 97–111.
Clogston, J., Craciun, G., Hart, D.J., Caffrey, M., 2005. Controlling release from the lipidic cubic phase by selective alkylation. J. Control. Release 102, 441–461.
Cui, J.X., Li, C.L., Wang, C.X., Li, Y.H., Zhang, L., Zhang, L., Xiu, X., Li, Y.F., Wei, N., 2011. Development of pegylated liposomal vincristine using novel slufobutyl ether cyclodextrin gradient: is improved drug retention sufficient to surpass DSPE-PEG-induced drug leakage? J. Pharm. Sci. 100, 2835–2848.
Cullis, P.R., Chonn, A., Semple, S.C., 1998. Interactions of liposomes and lipid-based carrier systems with blood proteins: relation to clearance behavior in vivo. Adv. Drug Deliv. Rev. 32, 3–17.
Daher, C.F., Baroody, G.M., Howland, R.J., 2003. Effect of a surfactant, Tween 80, on the formation and secretion of chylomicrons in the rat. Food Chem. Toxicol. 41, 575–582.
Dos Santos, N., Allen, C., Doppen, A.M., Anantha, M., Cox, K.A., Gallagher, R.C., Karlsson, G., Edwards, K., Kenner, G., Samuels, L., Webb, M.S., Bally, M.B., 2007. Influence of poly (ethylene glycol) grafting density and polymer length on liposomes: relating plasma circulation lifetimes to protein binding. Biochim. Biophys. Acta 1768, 1367–1377.
Efrat, R., Aserin, A., Kesselman, E., Danino, D., Wachtel, E., Garti, N., 2007. Liquid micellar discontinuous cubic mesophase from ternary monoolein/ethanol/water mixtures. Colloids Surf. A 299, 133–145.
Fjuskog, M.L., Frii, L., Bergh, J., 1994. Paclitaxel-induced cytotoxicity—the effects of cremophor EL (castor oil) on two human breast cancer cell lines with acquired multidrug resistant phenotype and induced expression of the permeability glycoprotein. Eur. J. Cancer 30, 687–690.
Gan, L., Han, S., Shen, J., Zhu, J., Zhu Chunliu Zhang, X., Gan, Y., 2010. Self-assembled liquid crystalline nanoparticles as a novel ophthalmic delivery system for dexamethasone: improving preocular retention and ocular bioavailability. Int. J. Pharm. 396, 179–187.
Garg, G., Saraf, S., Saraf, S., 2007. Cubosomes: an overview. Biol. Pharm. Bull. 30, 350–353.
Gaumet, M., Vargas, A., Gurny, R., Delie, F., 2008. Nanoparticles for drug delivery: the need for precision in reporting particle size parameters. Eur. J. Pharm. Biopharm. 69, 1–9.
Gelderblom, H., Verweij, J., Nooter, K., Sparreboom, A., 2001. Cremophor EL: the drawbacks and advantages of vehicle selection for drug formulation. Eur. J. Cancer 37, 1590–1598.
Giddi, H.S., Arunagirinathan, M.A., Bellare, J.R., 2007. Self-assembled surfactant nano-structures important in drug delivery: a review. Indian J. Exp. Biol. 45, 133–159.
Guo, C., Wang, J., Cao, F., Lee, R.J., Zhai, G., 2010. Lyotropic liquid crystal systems in drug delivery. Drug Discov. Today 15, 23–24.
Guo, M., Que, C., Wang, C., Liu, X., Yan, H., Liu, K., 2011. Multifunctional superparamagnetic nanocarriers with folate-mediated and pH-responsive targeting properties for anticancer drug delivery. Biomaterials 32, 185–194.
Higuchi, W.I., 1967. Diffusional models useful in biopharmaceutics:drug release rate processes. J. Pharm. Sci. 56, 315–324.
Johnsson, M., Barauskas, J., Norlin, A., Tiberg, F., 2006. Physicochemical and drug delivery aspects of lipid-based liquid crystalline nanoparticles: a case study of intravenously administered propofol. J. Nanosci. Nanotechnol. 6, 3017–3024.
Johnsson, M., Barauskas, J., Tiberg, F., 2005. Cubic phases and cubic phase dispersions in a phospholipid-based system. J. Am. Chem. Soc. 127, 1076–1077.
Kaasgaard, T., Drummond, C.J., 2006. Ordered 2-D and 3-D nanostructured amphiphile self-assembly materials stable in excess solvent. Phys. Chem. Chem. Phys. 8, 4957–4975.
Kim, S.C., Kim, D.W., Shim, Y.H., Bang, J.S., Oh, H.S., Wan Kim, S., Seo, M.H., 2001. In vivo evaluation of polymeric micellar paclitaxel formulation: toxicity and efficacy. J. Control. Release 72, 191–202.

Kossena, G.A., Charman, W.N., Boyd, B.J., Porter, C.J., 2004. A novel cubic phase of medium chain lipid origin for the delivery of poorly water soluble drugs. J. Control. Release 99, 217–229.
Lai, J., Chen, J., Lu, Y., Sun, J., Hu, F., Yin, Z., Wu, W., 2009. Glyceryl monooleate/poloxamer 407 cubic nanoparticles as oral drug delivery systems: I. In vitro evaluation and enhanced oral bioavailability of the poorly water-soluble drug simvastatin. AAPS Pharm. Sci. Technol. 10, 960–966.
Lee, J., Kellaway, I.W., 2000. In vitro peptide release from liquid crystalline buccal delivery systems. Int. J. Pharm. 195, 29–33.
Lee, K.W.Y., Nguyen, T.H., Hanley, T., Boyd, B.J., 2009. Nanostructure of liquid crystalline matrix determines in vitro sustained release and in vivo oral absorption kinetics for hydrophilic model drugs. Int. J. Pharm. 365, 190–199.
Lee, S.C., Kim, C., Kwon, I.C., Chung, H., Jeong, S.Y., 2003. Polymeric micelles of poly(2-ethyl-2-oxazoline)-block-poly((-caprolactone) copolymer as a carrier for paclitaxel. J. Control. Release 89, 437–446.
Li, S.D., Huang, L., 2008. Pharmacokinetics and biodistribution of nanoparticles. Mol. Pharm. 5, 496–504.
Liggins, R.T., Hunter, W.L., Burt, H.M., 1997. Solid-state characterization of paclitaxel. J. Pharm. Sci. 86, 1458–1463.
Maechling-Strasser, C., Déjardin, P., Galin, J.C., Schmitt, A., 1989. Preadsorption of polymers on glass and silica to reduce fibrinogen adsorption. J. Biomed. Mater. Res. 23, 1385–1393.
Markman, M., Kennedy, A., Webster, K., Kulp, B., Peterson, G., Belinson, J., 2011. Paclitaxel-associated hypersensitivity reactions: experience of the gynecologic oncology program of the Cleveland Clinic Cancer Center. J. Clin. Oncol. 18, 102–105.
Misiūnas, A., Talaikyte, Z., Niaura, G., Razumas, V., Nylander, T., 2008. Thermomyces lanuginosus lipase in the liquid-crystalline phases of aqueous phytantriol: X-ray diffraction and vibrational spectroscopic studies. Biophys. Chem. 134, 144–156.
Mori, Y., Nagaoka, S., Takiuchi, H., Kikuchi, T., Noguchi, N., Tnazawa, H., Noishiki, Y., 1982. A new antithrombogenic material with long polyethyleneoxide chains. Trans. Am. Soc. Artif. Intern. Organs 28, 459–463.
Müller, R.H., Jacobs, C., Kayser, O., 2001. Nanosuspensions as particulate drug formulations in therapy: rationale for development and what we can expect for the future. Adv. Drug Deliv. Rev. 47, 3–19.
Nguyen, T.H., Hanley, T., Porter, C.J., Larson, I., Boyd, B.J., 2010. Phytantriol and glyceryl monooleate cubic liquid crystalline phases as sustained-release oral drug delivery systems for poorly water soluble drugs I. Phase behaviour in physiologically-relevant media. J. Pharm. Pharmacol. 62, 844–855.
Orädd, G., Lindblom, G., Fontell, K., Ljusberg-Wahren, H., 1995. Phase diagram of soybean phosphatidylcholine–diacylglycerol–water studied by X-ray diffraction and ^{31}P- and pulsed field gradient ^{1}H-NMR: evidence for reversed micelles in the cubic phase. Biophys. J. 68, 1856–1863.
Otsuka, H., Nagasaki, Y., Kataoka, K., 2003. PEGylated nanoparticles for biological and pharmaceutical applications. Adv. Drug Deliv. Rev. 55, 403–419.
Patel, P.V., Patel, J.B., Dangar, R.D., Patel, K.S., Chauhan, K.N., 2010. Liquid crystal drug delivery system. Int. J. Pharm. Appl. Sci. 1, 118–123.
Riviere, K., Huang, Z., Jerger, K., Macaraeg, N., Szoka Jr., F.C., 2011. Antitumor effect of folate-targeted liposomal doxorubicin in KB tumor-bearing mice after intravenous administration. J. Drug Target. 19, 14–24.
Rizwan, S.B., Assmus, D., Boehnke, A., Hanley, T., Boyd, B.J., Rades, T., Hook, S., 2011. Preparation of phytantriol cubosomes by solvent precursor dilution for the delivery of protein vaccines. Eur. J. Pharm. Biopharm. 79, 15–22.
Rizwan, S.B., Hanley, T., Boyd, B.J., Rades, T., Hook, S., 2009. Liquid crystalline systems of phytantriol and glyceryl monooleate containing a hydrophilic protein: characterisation, swelling and release kinetics. J. Pharm. Sci. 98, 4191–4204.
Rosenbaum, E., Tavelin, S., Johansson, L.B., 2010. A characterisation study on the application of inverted lyotropic phases for subcutaneous drug release. Int. J. Pharm. 388, 52–57.
Song, S., Liu, D., Peng, J., Deng, H., Guo, Y., Xu, L.X., Miller, A.D., Xu, Y., 2009. Novel peptide ligand directs liposomes toward EGF-R high-expressing cancer cells. FASEB J. 23, 1–9.
Tiberg, F., Fredrik, J., 2010. Lipid liquid crystals for parenteral sustained-release applications: combining ease of use and manufacturing with consistent drug release control. In: Injectable Drug Delivery 2010: Formulations Focus [C]. Frederick Furness Publishing, pp. 9–12.
Weiss, R.B., Donehower, R.C., Wiernik, P.H., Ohnuma, T., Gralla, R.J., Trump, D.L., Baker Jr., J.R., Van Echo, D.A., Von Hoff, D.D., Leyland-Jones, B., 1990. Hypersensitivity reactions from Taxol. J. Clin. Oncol. 8, 1263–1268.
Wen, Z., Yan, Z., Hu, K., Pang, Z., Cheng, X., Guo, L., Zhang, Q., Jiang, X., Fang, L., Lai, R., 2011. Odorranalectin-conjugated nanoparticles: preparation, brain delivery and pharmacodynamic study on Parkinson's disease following intranasal administration. J. Control. Release 151, 131–138.
Woodle, M.C., Lasic, D.D., 1992. Sterically stabilized liposomes. Biochim. Biophys. Acta 1113, 171–199.
Wörle, G., Drechsler, M., Koch, M.H., Siekmann, B., Westesen, K., Bunjes, H., 2007. Influence of composition and preparation parameters on the properties of aqueous monoolein dispersions. Int. J. Pharm. 329, 150–157.
Yaghmur, A., Glatter, O., 2009. Characterization and potential applications of nanostructured aqueous dispersions. Adv. Colloid Interface Sci. 147–148, 333–342.
Yaghmur, A., Michael, R., 2010. Liquid crystalline nanoparticles as drug nanocarriers. In: Fanun, M. (Ed.), Colloids in Drug Delivery. CRC Press, London, pp. 337–353.
Yang, D., Armitage, B., Marder, S.R., 2004. Cubic liquid-crystalline nanoparticles. Angew. Chem. Int. Ed. Engl. 43, 4402–4409.
Yao, H.J., Ju, R.J., Wang, X.X., Zhang, Y., Li, R.J., Yu, Y., Zhang, L., Lu, W.L., 2011. The antitumor efficacy of functional paclitaxel nanomicelles in treating resistant breast cancers by oral delivery. Biomaterials 32, 3285–3302.